Numerical Simulation and Analysis of a Prefrontal Squall Line. Part I: Observations and Basic Simulation Results

JENNIFER M. CRAM, ROGER A. PIELKE, AND WILLIAM R. COTTON

Department of Atmospheric Science, Colorado State University, Fort Collins, Colorado

(Manuscript received 16 November 1990, in final form 10 June 1991)

ABSTRACT

An observational and numerical study of the squall line that occurred on 17–18 June 1978 is presented. This squall line was initially triggered by the strong surface convergence along a cold front and stretched from Illinois to the Texas Panhandle. The squall line was aligned with the surface front during its initial development (at 0000 UTC 18 June 1978), but then propagated faster than the front, resulting in a separation of approximately 200 km by 0300 UTC and 300–400 km by 0600 UTC. The Colorado State University (CSU) Regional Atmospheric Modeling System (RAMS) is used to model the squall-line development and propagation. Results are described from several experiments that tested the sensitivity to the use of the Kuo-type cumulus parameterization scheme and grid-scale microphysical processes. The simulations that included the cumulus parameterization scheme accurately modeled the initial development of the squall line and its subsequent movement away from the front.

1. Introduction

Squall lines are most simply defined as lines of convection. These lines can be only 100 km long or extend to nearly 1000 km. There is a distinct linear structure to squall lines (as compared to individual thunderstorm cells or systems), although the lines do not necessarily propagate or translate in a direction perpendicular to their length. As Bluestein and Jain (1985) point out, squall lines may be oriented along a front for part of or all of their lifetimes, or not at all. Bluestein and Jain's general definition of a squall line as a line-oriented mesoscale convective system (Maddox 1980) will be adopted in this study.

The numerical modeling of squall lines has only recently been extended to three dimensions from two dimensions because of a relaxation of computer memory and speed limitations. The linear shape of squall lines has implied that they may perhaps be adequately modeled in only two dimensions. However, the interactions between synoptic-scale features (such as frontal forcing) and mesoscale features (such as a squall line and gravity waves) are often difficult to model in only two dimensions, with initialization of the model from only one sounding. Even with current computer power, it is difficult to have a large enough domain (several thousands of kilometers) with a small enough resolution (tens of kilometers or even smaller) to adequately resolve the meso-β- and meso-γ-scale processes internal to, and in the vicinity of, a squall line, and at the same time also properly simulate the synoptic- and meso-α-scale processes that initially force the squall line and may continue to interact with it. There are several different scales of motion that can be responsible for forcing squall-line development and propagation; it is impossible to correctly model all of these scales with current computer power. As a result, the modeling of squall lines has split into two widely separate schools. One group approaches the problem with the finest resolution possible, but then has to neglect larger-scale processes. The other group approaches the problem with synoptic- and meso-α-scale resolutions but then has to neglect or parameterize the effects of deep convection.

Most higher-resolution squall-line modeling studies (with grid spacings from 500 m to 5 km) have been two-dimensional and initialized in a "horizontally homogeneous" manner that is, from one sounding and an initial forcing of some sort such as a warm bubble, convergent circulation, or cold pool (Hane 1973; Moncrieff and Miller 1976; Thorpe et al. 1982; Hane et al. 1987; Nicholls 1987; Nicholls and Weissbluth 1988; Nicholls et al. 1988; Rotunno et al. 1988; Lafore and Moncrieff 1989; Tripoli and Cotton 1989a,b; Schmidt and Cotton 1990). Such studies are suitable for investigating the internal cloud-scale squall-line dynamics and convective heating effects and the cloud-scale influence on the meso-β-scale aspects of squall-line propagation and maintenance (such as the importance of strong downdrafts and the gust front). However, they are unable to take three-dimensional

Corresponding author address: Dr. Jennifer Cram, Department of Atmospheric Science, Colorado State University, Fort Collins, CO 80523.

and synoptic-scale variations into account or interactions with other mesoscale features (such as fronts) that may have initially forced the squall line.

The larger-scale studies that have been initialized with synoptic data generally have grid spacings on the order of 25–100 km and concentrate on the synoptic- (>2000 km) and meso-α- (200–2000 km) scale aspects of squall-line propagation and maintenance (Chang et al. 1981; Orlanski and Ross 1984, 1986; Zhang and Fritsch 1986, 1987, 1988a,b; Zhang et al. 1988, 1989; Zhang and Gao 1989). However, these studies are generally unable to resolve the meso-β- and meso-γ-scale processes that may be important in the development and propagation of squall lines. An additional problem with larger-scale studies is their need to rely on parameterizations of subgrid-scale processes. In some instances these parameterizations may incorrectly force grid-scale motions or mechanisms. For instance, Tripoli and Cotton (1989b) noted that the inclusion of a convective parameterization incorrectly coupled convective activity with the motion of a large-scale gravity wave. A smaller-scale simulation with explicit convective processes did not couple the convective activity and the gravity wave motion.

The purpose of this study is to investigate the development and propagation of a prefrontal squall line that occurred during 17–18 June 1978. This is a case with relatively weak upper-air forcing that produced a very long, prefrontal squall line. A nested grid version of the Regional Atmospheric Modeling System (RAMS) developed at Colorado State University is used to simulate the development of the squall line across several scales, from the synoptic scale down to meso-β scales. A coarse grid (80-km grid spacing) is used to simulate the synoptic-scale dynamics and frontal forcing. A finer mesh grid (20-km grid spacing) is needed to represent the separation of the squall line from the front. The squall line initially developed along the strong surface frontal convergence line, but then moved out ahead of the front in both the observations and modeling simulations. In Cram et al. (1991, hereafter referred to as Part II), it will be shown that the squall line propagated as an internal gravity wave in the modeled simulation. The speed of the propagating wave was greater than that of the front, resulting in the separation with time of the front and squall line, and the "prefrontal" character of the squall line. The gravity wave and squall line appear to be manifestations of a wave–CISK-type process.

The observational analysis of the squall line is presented in this paper, as is a brief description of the numerical methods and data used in the simulations. Results from model simulations with 80-km and 20-km grid spacings are discussed and compared to the observational data. Several sensitivity studies were completed to investigate the importance of the parameterized and grid-resolved moist thermodynamics, including latent heat release, phase changes of water, and microphysical processes. The hypothesized mechanism of the squall-line propagation as an internal gravity wave is discussed in Part II, as well as an unsuccessful attempt to model the squall line with a 5-km grid mesh.

2. Case description

The case chosen for this study is that of a midlatitude squall line that developed on 17–18 June 1978. This case was observed during project NIMROD (Northern Illinois Meteorological Research on Downbursts; Fujita 1981) and was used for a Doppler radar study by Srivastava et al. (1986). The squall-line convection initially developed along a very long, well-defined cold front, and then moved out ahead of, and away from, the front, thus giving the squall line its "prefrontal" character. At its peak, a line of convection extended all the way from Illinois to the Texas Panhandle.

Srivastava et al. (1986) studied a portion of the trailing anvil region associated with the squall line. They described the synoptic situation for this case as consisting of low-level warm advection from the southwest at 850 mb with cold advection aloft at 700 and 500 mb. From radar reflectivity pictures they determined that individual cores in the squall line had lifetimes of 30–40 minutes and moved northeastward, while the line itself moved southeastward as new convective elements formed up to 25 km ahead of the line. Srivastava et al. noted that the squall line began to intensify rapidly at 2130 UTC (1530 Local Standard Time), and by 0100 UTC had formed a continuous cloud band stretching 2000 km from Wisconsin to Texas, with widths ranging from 70 to 200 km. The squall line moved southeastward through northern Illinois at approximately 15 m s^{-1}, "considerably faster than the motion of the cold front." According to their observations, the squall line passed through their network between 0200 UTC 17 June and 0800 UTC 18 June, while the cold front did not pass through until 1200 UTC 18 June. Figures 1a and 1b show the satellite imagery of the squall line at 0100 and 0430 UTC. At 0100 UTC the squall line had widened to almost 200 km and at 0430 UTC was more than 300 km wide.

Several points need to be noted on the relation of the Srivastava et al. (1986) paper to this study. First of all, their study mainly concentrated on a semidetached portion of the trailing anvil of the squall line, while most of the emphasis in this study is on the leading convective region of the squall line and its propagation. It is also not known (nor addressed by Srivastava et al.) to what extent the observations at the northern edge of the squall line, where the NIMROD network was situated, are representative of the entire length of the squall line. Whereas the squall line stretched from Illinois to the Texas Panhandle, the NIMROD field project was only situated in northern Illinois, at the very northern end of the squall line. The northern end of the squall-line convection seemed to

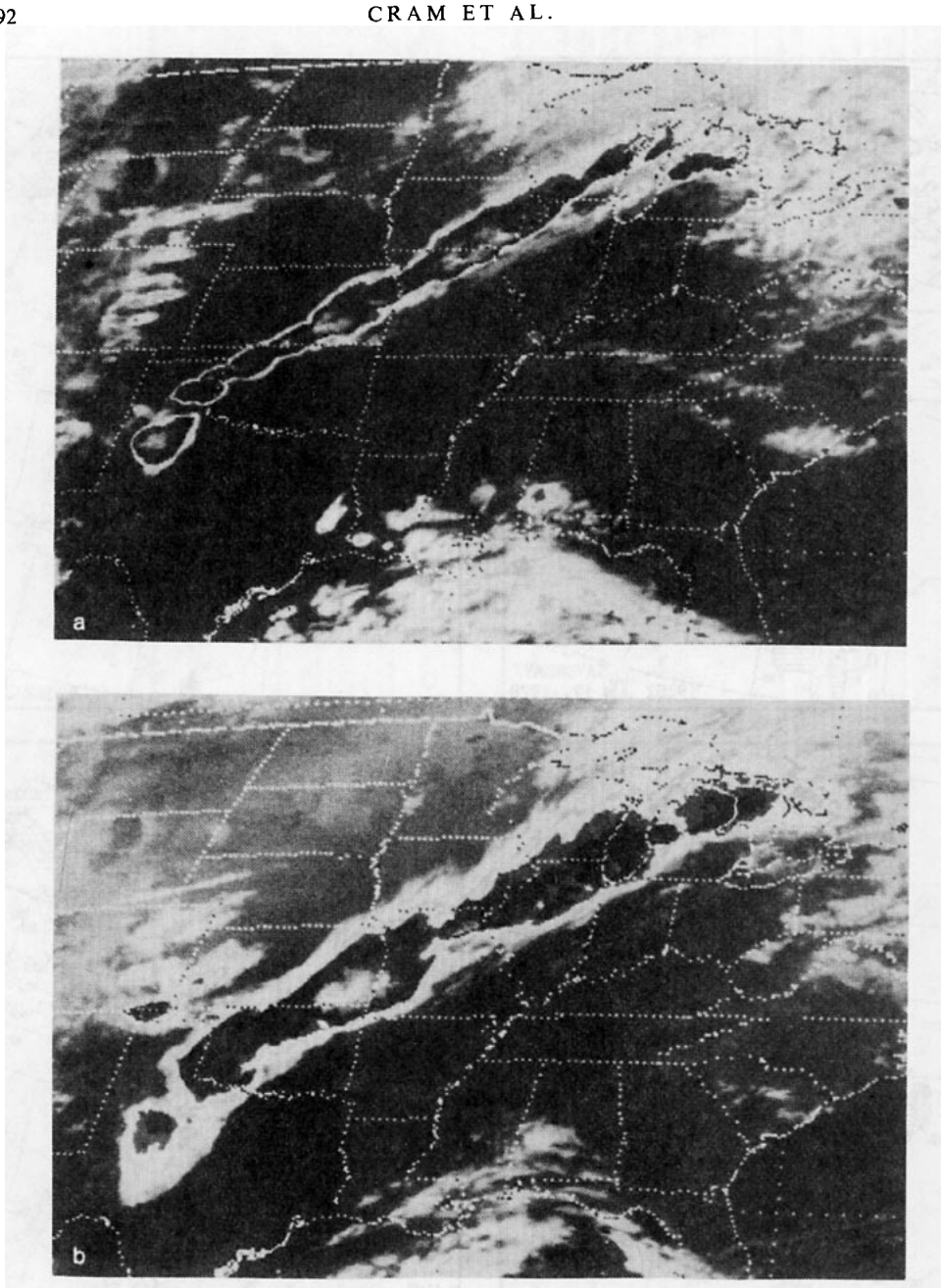

FIG. 1. Satellite imagery of a squall line at (a) 0100 UTC 18 June 1978 and (b) 0430 UTC 18 June 1978 (from Srivastava et al. 1986).

merge with a large, nonlinear in shape, mesoscale convective system, (MCS, Fig. 2) so it is not clear whether the mechanisms operating in that region apply to the full length of the squall line.

Thomas Matejka (personal communication) participated in the field project that observed this squall line in northern Illinois and provided several observations of it. First of all, he emphasized the discrete nature of the squall-line propagation. He noted that new thunderstorms formed 20–35 km ahead of the forward edge of the gust front and that the actual passage of the gust front was associated with dissipating elements of the squall line. In northern Illinois, he observed the frontal passage approximately 4 h after the passage of the rear edge of the trailing stratiform precipitation. Matejka also noted a much larger discrete jump of the squall line. He observed that the squall line dissipated in northern Illinois before reaching the Yorkville field site and then reformed 100 km ahead of the old position. He noted that the radar data showed that the squall line seemed to consist of "large segments, 100 to 200 km long, that marched along in phase, oc-

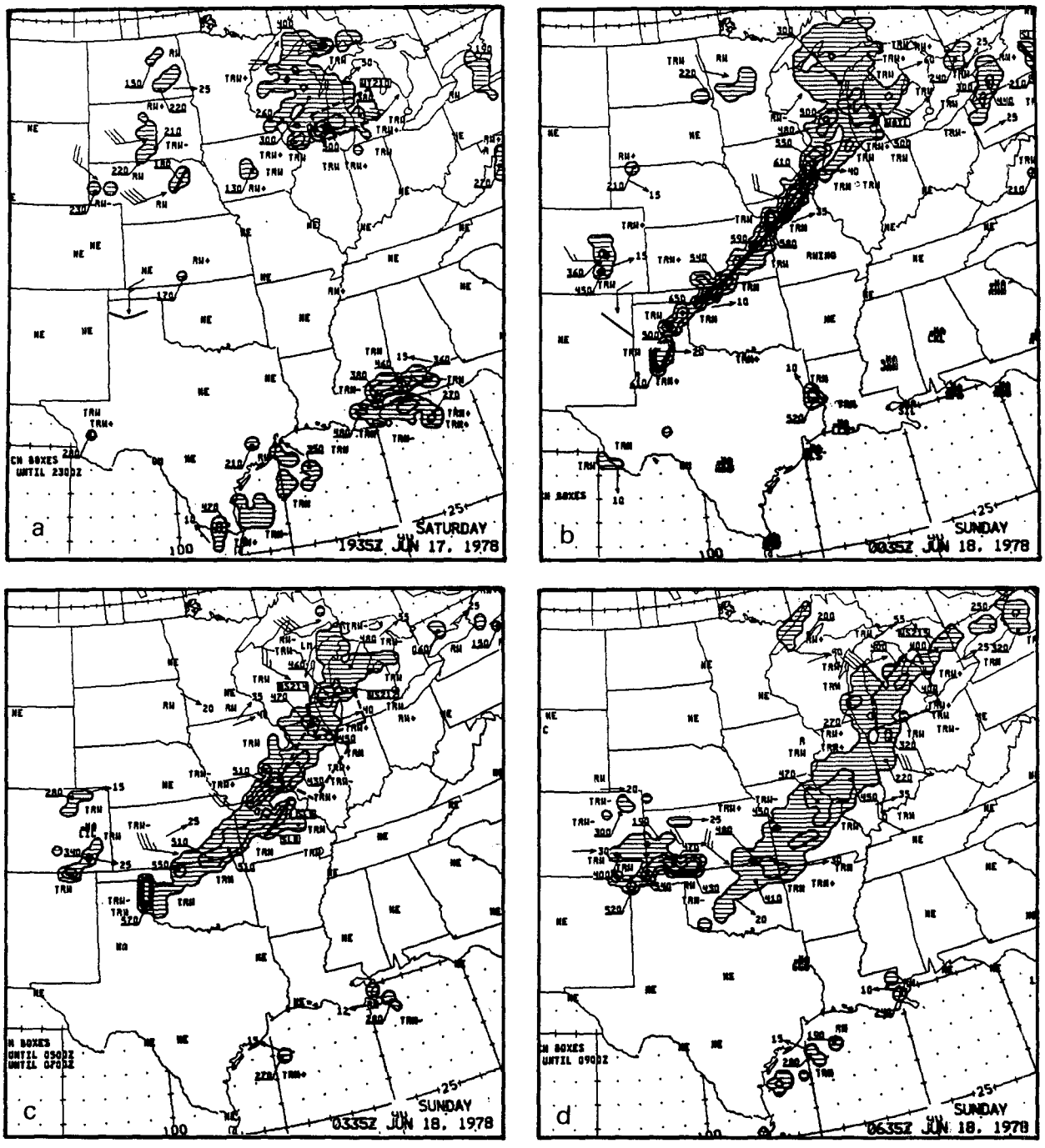

FIG. 2. Radar summary charts at (a) 1935 UTC 17 June 1978, (b) 0035 18 June 1978, (c) 0335 UTC 18 June 1978, and (d) 0635 UTC 18 June 1978.

casionally jumping forward but eventually getting back in step with adjacent segments."

Figure 2 shows the radar summary charts from the National Weather Service at 1935 UTC 17 June and 0035, 0335, and 0635 UTC 18 June. The first echoes associated with the squall line were visible at 1935 UTC (Fig. 2a). A small echo over southern Kansas and another over central Iowa were the first indications of the developing squall line. By 0035 UTC (Fig. 2b) the line of radar echoes was continuous from the Texas Panhandle through northern Illinois. The maximum tops reported at that time were all near 60 000 feet (18 km), although one top in the Texas Panhandle extended to 65 000 feet (almost 20 km). The movements of individual cells along the line range from 10 to 40 kt (5 to 20 m s^{-1}) and were generally eastward. At 0035 UTC

the line was fairly straight and continuous; there was no evidence on that scale of a discrete or segment-like propagation.

From 0035 through 0335 UTC (Figs. 2b,c) the line translated approximately 100–300 km southeastward. Individual cell movements along the leading edge of the line varied from 25 to 40 kt (13–20 m s^{-1}) and were eastward through northeastward. Evidence of the discrete propagation of the line is visible at 0335 UTC (Fig. 2c). A segment of convection approximately 150 km long appears to have developed approximately 50 km ahead of the original line over central Missouri. The large area of convection associated with the MCS decreased during this period, and by 0335 UTC the squall line and remaining MCS activity formed a continuous and fairly straight line of radar echoes from the Texas Panhandle to the northern edge of Lake Michigan. Between 0335 and 0635 UTC, the radar echoes associated with the squall line widened and weakened. The width of the squall-line echo region increased from approximately 150 km at 0335 UTC (Fig. 2c) to 200 km at 0635 UTC (Fig. 2d). The individual echoes moved at speeds from 25 to 30 kt eastward through southeastward during this period. From 0635 to 0935 UTC (not shown) the squall line continued to weaken.

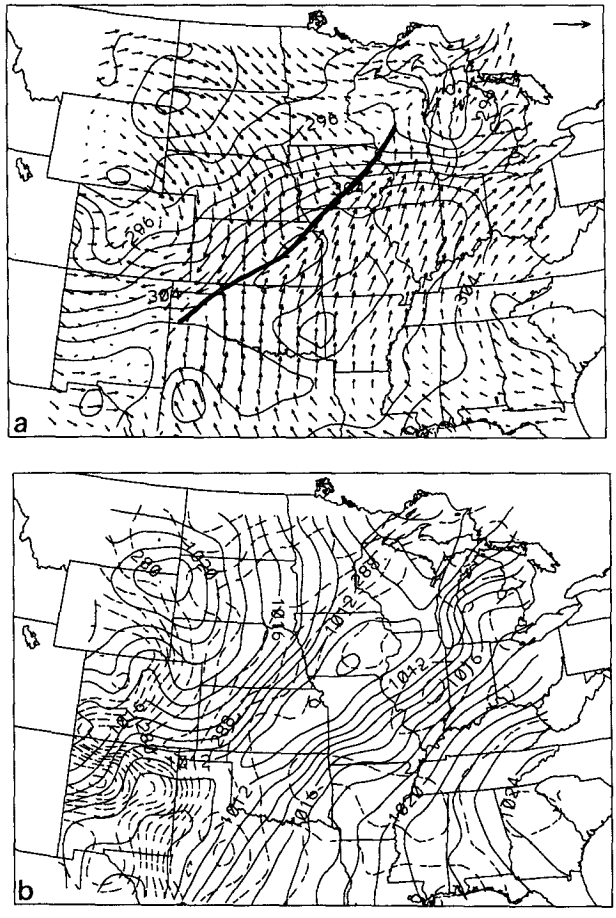

FIG. 3. Surface analyses at 2100 UTC 17 June 1978 for (a) wind vectors and temperature (K, contour interval is 2 K); and (b) MSLP (solid lines, mb, contour interval is 1 mb) and dewpoint temperature (dashed lines, contour interval is 2 K). The vector lengths are scaled by speed: the single vector in the upper right corner of (a) represents 15 m s^{-1}. The maximum wind speeds in (a) are 10 m s^{-1}. The solid line superimposed on (a) is the frontal position.

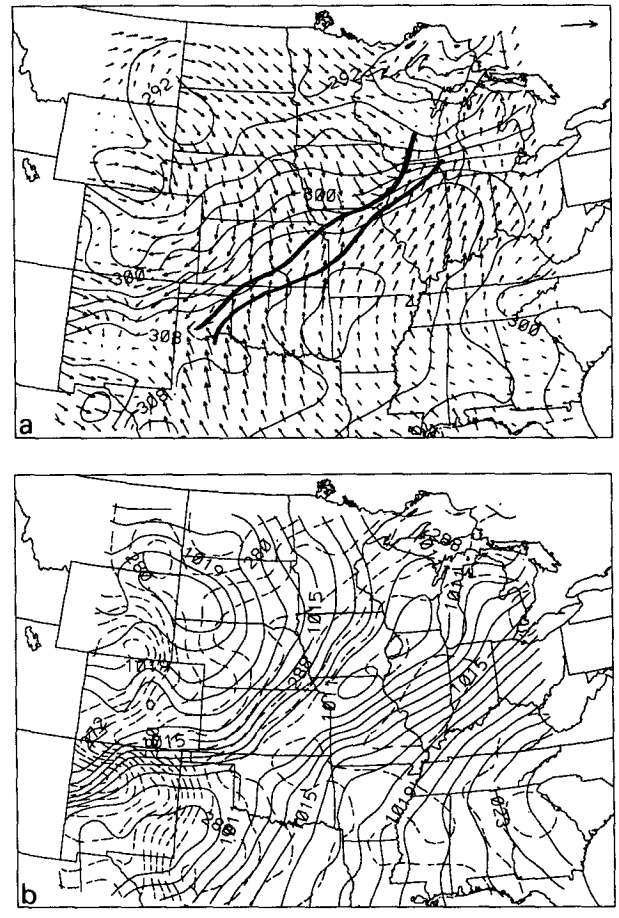

FIG. 4. Same as Fig. 3, except at 0000 UTC 18 June 1978. The solid lines superimposed on (a) are the frontal position (farther northwest) and the leading edge of the radar echoes at 0035 UTC 18 June (farther southeast).

Surface analyses of winds, temperature, mean sea level pressure (MSLP), and dewpoint temperature are shown in Figs. 3–6 for 3-h intervals from 2100 UTC 17 June through 0600 UTC 18 June. The data and analysis method are described more thoroughly in Cram (1990). The North American hourly surface synoptic observation dataset available on the NCAR data archives was used for these analyses.

Figure 3 shows the surface analyses at 2100 UTC, as the squall-line convection was just developing. At this time the wind shift line was aligned almost exactly along the center of the pressure trough, and there was a strong temperature gradient to the northwest of the line. The wind shift line was also aligned along the leading edge of a gradient in dewpoint temperature.

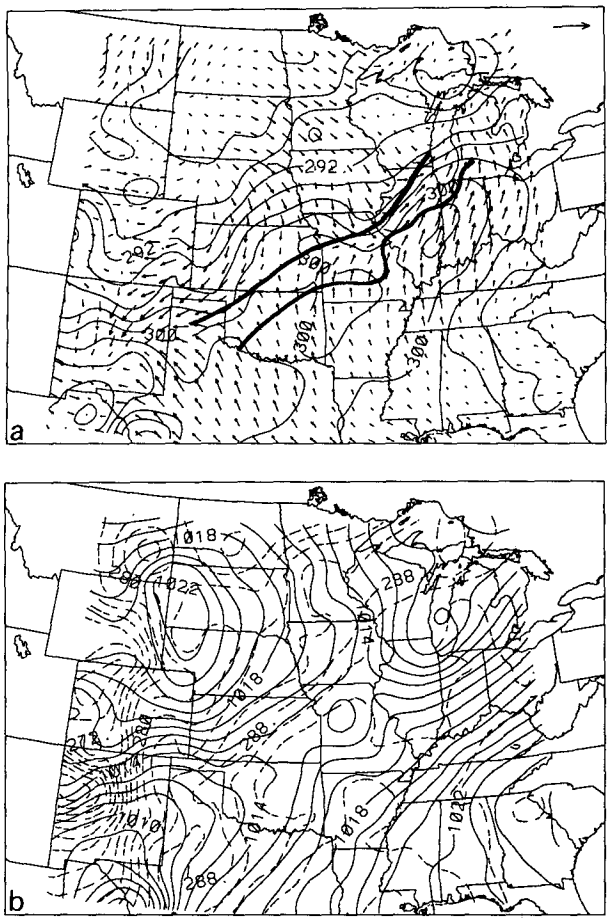

FIG. 5. Same as Fig. 3, except at 0300 UTC 18 June 1978. The solid lines superimposed on (a) are the frontal position (farther northwest) and the leading edge of the radar echoes at 0335 UTC 18 June (farther southeast).

The cold front is most clearly defined by the wind shift line.

The squall-line convection first started to appear in the radar and satellite imagery between 1900 and 2100 UTC, and the line was continuous by 2300–2400 UTC. The leading edge of the echoes on the radar summary chart for 0035 UTC are superimposed on the surface analyses at 0000 UTC (Fig. 4) and are essentially aligned along the wind shift line at these times. There is a widening separation between the wind shift line and the leading edge of the radar echoes by 0300 UTC (Fig. 5). After 0300 UTC it becomes increasingly difficult to define the frontal position from the surface wind and temperature analyses because of the convective-related perturbations. Although the leading edge of the radar echoes is used to define the leading edge of the squall line in this study, one reviewer correctly pointed out that range effects (elevated radar beam height and beam broadening at far ranges) may lead to significant error and that the depicted edge may actually reflect leading-anvil overhang. Even though it is impossible to define exactly where the leading edge of the squall-line convection is, the 200-km separation of the front and squall-line convection (leading edge of radar echoes) by 0300 UTC is much larger than such range effect errors would be.

The standard hourly surface synoptic observations were used to produce the analyses in Figs. 3–6. It is very difficult (perhaps impossible) to accurately analyze convectively induced wind shifts from such observations. Therefore, the lack of evidence of gust front convergences in the hourly surface analyses is certainly not proof of the lack of a gust front. However, the hourly surface analyses do clearly show the frontal position and movement, and in conjunction with the radar summary charts show the increasing separation of the front and squall-line convection.

Some insight into the relative positions of the front and squall-line convection can be gained by more closely analyzing the MSLP analyses. The front appears to be consistently aligned behind the surface pressure minimum. Although there are transient perturbations in the surface temperature analyses, the frontal temperature gradient is also most consistently aligned along the back edge of the pressure trough. Before the squall-

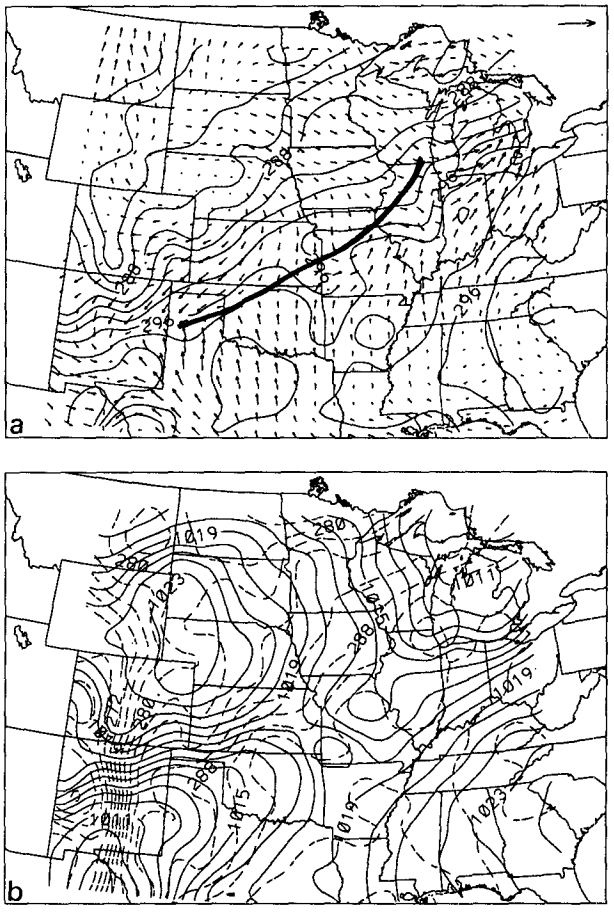

FIG. 6. Same as Fig. 3, except at 0600 UTC 18 June 1978. The solid line superimposed on (a) is the frontal position.

line convection has significantly developed (before 2300 UTC 17 June 1978), the surface pressure trough remains relatively narrow and well defined. The wind shift line is aligned along the center of the trough throughout this period. Between 1200 and 1800 UTC the minimum pressures in the center of the trough increase from approximately 1005 to 1009 mb, and then stay at that level through 2400 UTC. Between 0000 and 0300 UTC the trough widens and the minimum pressures increase to 1014 mb. The pressures continue to increase and the trough widens through 0600 UTC. At times beyond 0000 UTC the leading edge of the squall-line convection is aligned ahead of the surface pressure minimum, and the most consistent analysis of the frontal position appears to be behind the surface pressure minimum. By 0300 UTC this results in a separation distance between the front and the leading edge of the squall line of approximately 200 km. By 0600 UTC this gap appears to be approximately 250–300 km, although the squall-line convection is not very active at this time.

Figure 7 shows the surface analysis of 12-h precipitation at 1200 UTC 18 June 1978. There was not any observed precipitation associated with the squall line at 0000 UTC, although the precipitation analyses were based on a much more limited number of stations than the other surface data analyses.

The National Meteorological Center (NMC) spectral model upper-air analyses (2.5° grid spacing) were discussed in Cram (1990). To summarize, the surface front was oriented just ahead of a low-level trough, with strong warm advection occurring ahead of the trough up to 5.0 km. The flow above that level was generally barotropic and with a more westerly component. There were no significant upper-level jets resolved by the NMC spectral data along or through the frontal zone.

Presquall rawinsonde sounding data from OKC (Oklahoma City, Oklahoma) is shown in Fig. 8. At 0000 UTC 18 June, OKC was still ahead of the squall line. A low-level stable layer existed below 750 mb at

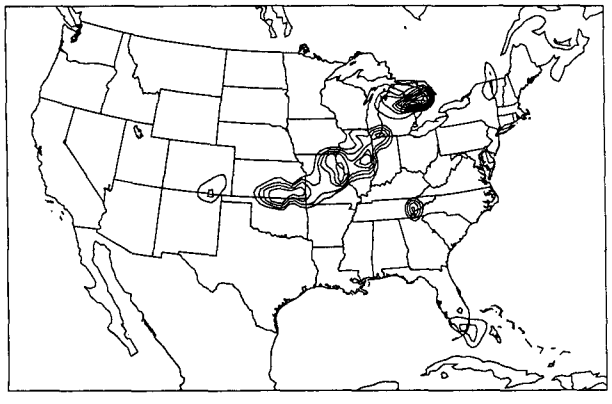

FIG. 7. Surface analysis of 12-hour precipitation (contour interval is 0.5 cm) at 1200 UTC 18 June 1978.

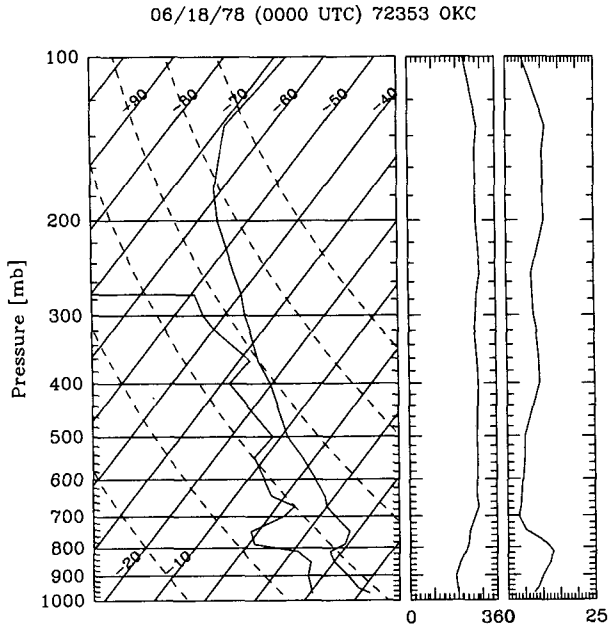

FIG. 8. OKC rawinsonde sounding at 0000 UTC 18 June 1978. Temperature and dewpoint are shown on the left panel, and wind direction (direction wind is blowing from in degrees) and speed (m s^{-1}) are shown in the two farthest right panels.

both 1200 UTC 17 June and 0000 UTC 18 June, with a deep layer of conditional instability above (conditionally unstable with respect to a surface parcel). There is very little wind shear, except in a layer below 700 mb. The surface winds are approximately 8 m s^{-1} from 200°, while the 700-mb winds are approximately 5–10 m s^{-1} from 280°. Above 700 mb there is much less speed and directional shear. The UMN (Monett, Missouri), TOP (Topeka, Kansas), and PIA (Peoria, Illinois) soundings all show similar characteristics. The existence of the low-level stable layer below 750 mb is important in inhibiting the convection until the frontal forcing becomes strong. The representation of this low-level stable layer in the model initial analyses was found to be critical to the proper development of the convection along the front. The existence of weak vertical shear is consistent with Bluestein and Jain's (1985) "broken-line" squall-line composite classification. In their study, the broken-line classification is that associated with frontal-type squall lines and most closely represents the squall line in this study. They point out that this sort of weakly sheared environment for squall lines is indicative of strong external forcing for the squall line, such as by frontal convergence.

To summarize, the squall line developed explosively between 2100 and 0000 UTC. The upper-air and surface analyses show that the squall line was primarily forced by strong surface frontal convergence, with very weak flow aloft. The soundings indicate that the squall line developed in a conditionally unstable environment with a low-level stable area ahead of the front that

helped to inhibit convection ahead of the front and squall line. The vertical wind profiles in the presquall environment are similar to those described by Bluestein and Jain (1985) for prefrontal-type squall lines. The hourly surface analyses show that the squall line initially developed along the front, but by 0300 UTC had moved almost 200 km ahead of the front. The widening and filling of the trough is associated with the convectively modified air (surface mesohigh region) behind the squall line. The active convection in the squall line appears to have lasted from approximately 2100 UTC 17 June to between 0300 and 0600 UTC 18 June, with an area of stratiform precipitation remaining at 0600 UTC.

It is impossible to conclusively determine the mechanism of the squall-line propagation from the analyses of the hourly surface synoptic observations. Srivastava et al. (1986) and Matejka (personal communication) report observations of the squall line propagating and developing independently of the gust front, although such motions are not resolvable from the hourly surface observations. Overall, the hourly surface analyses and observations are inconclusive as mechanisms of the squall-line propagation in this case. There is no clear indication of gust front processes, although such processes would not necessarily be resolvable in the hourly observations. The modeling study was thus carried out as an attempt to determine the propagation mechanism for the 17–18 June squall line.

3. Model description

a. Datasets

The standard datasets used in the RAMS initial data analysis package are available on, or derived from, the National Center for Atmospheric Research (NCAR) data archives and are described in Cram (1990). These include the NMC spectral model analyses, the NMC rawinsonde data, the NMC 3-h surface data, the 30′ resolved terrain and land versus water data, and the 1° resolved sea surface temperature data. Special datasets used in this study also included hourly surface data.

b. Formulation of RAMS initial analysis package

The objective analysis and initialization package is used to create the initial and lateral boundary conditions used in the model. The initial analysis package was first developed by Tremback (1990), although many modifications and additions have been added by other users. The package is described in detail in Cram (1990). The analysis is hydrostatic and performed on isentropic surfaces. A Barnes (1964, 1973) objective analysis scheme is applied, and the user can input parameters that will determine the characteristics of the response function for the scheme. There is no imposed balance between the wind and mass field analyses.

TABLE 1. Basic formulation of the RAMS model.

CSU RAMS Colorado State University Regional Atmospheric Modeling System
• Staggered C grid (Arakawa and Lamb 1981), lat–long coordinates.
• Terrain-following σ_z vertical coordinate system, transformation as described in Gal-Chen and Somerville (1975a,b) and Clark (1977).
• Nonhydrostatic.
• Leapfrog time-differencing, second-order advection.
• Rayleigh friction layer at top (Cram 1990).
• Two-way interactive nesting (Clark and Farley 1984).
• Surface energy budget, soil model (Mahrer and Pielke 1977; McCumber and Pielke 1981; Tremback and Kessler 1985).
• Radiation parameterization (Mahrer and Pielke 1977). Other option of Chen and Cotton (1983a,b) also used for one experiment.
• Deformation K closure turbulence parameterization (Smagorinsky 1963; Lilly 1962; Hill 1974; Tripoli and Cotton 1982; Tremback 1990).
• Grid-scale microphysics with prognostic equations for rain, ice, and snow mixing ratios (Cotton et al. 1982, 1988; Flatau et al. 1989).
• Modified Kuo-type cumulus parameterization, downdraft option (Kuo 1965, 1974; Molinari 1985; Tremback 1990).
• Time-dependent lateral boundary conditions (Davies 1976; Davies and Turner 1977; Davies 1983).
• Initial analysis from NMC spectral model, rawinsonde data, surface data (Tremback 1990; Cram 1990).

c. Model formulation/options

The model used in this study was the Regional Atmospheric Modeling System (RAMS) (Tremback et al. 1986; Cotton et al. 1988) developed at Colorado State University. The basic formulation of the RAMS model used in this study is outlined in Table 1. The specific version of the model used was 2A. The options used in these simulations included two-way interactive nesting, nonhydrostatic, time-splitting, a cumulus parameterization scheme, warm-rain and ice-phase microphysics, a surface parameterization, a radiation parameterization, and time-dependent lateral boundary conditions. The convective parameterization is a modified form of the Kuo-type parameterizations of Kuo (1965, 1974) and Molinari (1985) developed by Tremback (1990). Modifications include a simple downdraft calculation and the calculation of the b parameter based on the precipitation efficiency formula in Fritsch and Chappell (1980a). A modified form of Rayleigh friction was developed to be used in association with the "wall on top" top boundary condition. This form of Rayleigh friction relaxes the model variables toward a spatial moving-average value. The Rayleigh friction layer in these simulations is applied in the 15–20-km layer. A more detailed description of the model is provided in Cram (1990).

4. Control and sensitivity experiments

The nested grid (20-km grid spacing) simulations are described in this section. The model domain and resolution for the simulations are briefly outlined, and

the results from the different simulations are then described and analyzed.

a. Simulation parameters

The simulations described had the same coarse and fine mesh domains, but differed in their inclusions of the explicit microphysics and the cumulus parameterization scheme. The large-scale areas covered 50° × 30° with a grid spacing of 1.0° × 0.75° (approximately 80 km at 40°N), or 50 × 41 points in the horizontal. There were 32 vertical grid levels. The vertical grid spacing varied from 250 m at the surface to 800 m at the top of the model (approximately 20 km). A Rayleigh friction layer extended from 15 to 20 km. A large time step of 120 seconds was used. The model terrain and horizontal domain are shown in Fig. 9. The nested grid in these simulations has a ratio of 1:4 (20-km grid spacing) over an area that covers about half of the north–south extent of the squall line (20° × 13°, 80 × 52 horizontal grid points). The vertical spacing is the same as on the large scale (32 levels). The nested domain is also shown in Fig. 9.

The initial fields for these simulations (on the 80-km grid) were obtained by using the analysis scheme described in section 3b. The model was initialized at 1200 UTC 17 June 1978. The coarse grid only was run to 1800 UTC, when the nested grid was added. The four simulations to be discussed will be referred to as:

DRY: Included neither cumulus parameterization nor explicit microphysics, and no latent heating effects.

MIC: Included explicit microphysics but no cumulus parameterization.

CU: Included cumulus parameterization but no explicit microphysics, except that latent heat is released with grid-scale condensation and production of cloud water.

ALL: Included both cumulus parameterization and explicit microphysics.

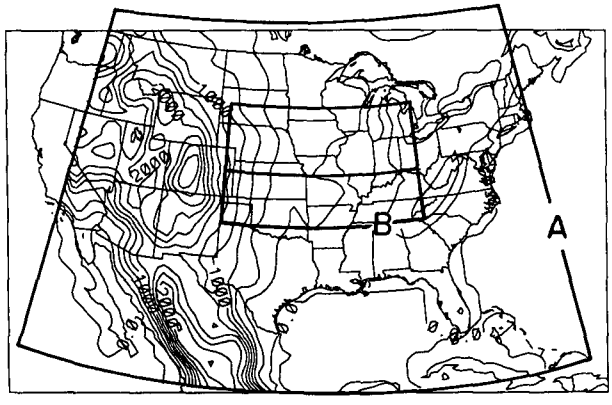

FIG. 9. Model terrain and horizontal domains of coarse (Box A) and fine (Box B) mesh grids. The horizontal line through Box B is the location for all vertical cross sections shown in this section.

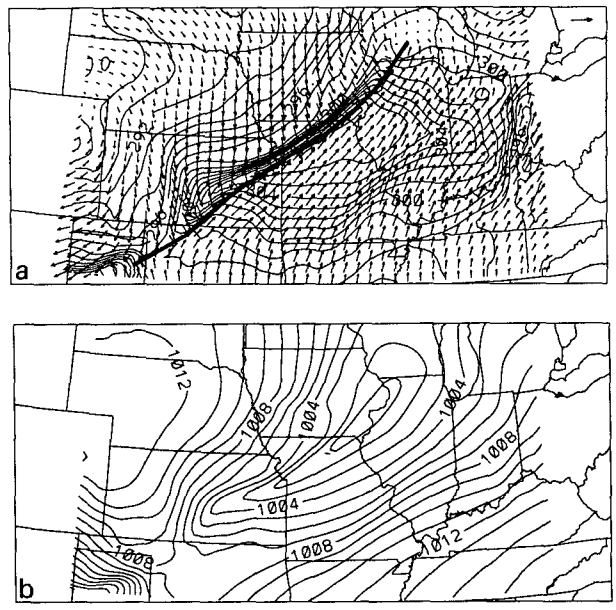

FIG. 10. Surface analyses from DRY simulation at 0300 UTC 18 June 1978 of (a) horizontal winds and temperature (contour interval is 1 K) and (b) reduced MSLP (contour interval is 1 mb). The lengths of the vectors in (a) are proportional to the speed: the vector in the upper-right corner of (a) is 20 m s^{-1}. The frontal position is superimposed on (a).

All of the figures and discussion in the following section will be concerned with the simulations on the 20-km mesh nested grid. The ALL simulation will be described in the greatest detail, with only brief discussions of the DRY, MIC, and CU simulations. Because of the model resolution (20-km grid spacing), the inclusion of a cumulus parameterization is necessary to simulate any convective effects. The DRY and MIC simulations were thus included only as points of comparison with the ALL and CU simulations.

b. Comparison of effects of inclusion of microphysics and cumulus parameterization

1) DRY SIMULATION

Figure 10 shows the surface analyses from the DRY simulation of horizontal winds and temperature and reduced MSLP at 0300 UTC 18 June (4–6 hours into the lifetime of the observed squall line). The position of the surface front is superimposed on the wind analyses. The frontal movement from 2100 UTC 17 June through 0600 UTC 18 June in the DRY simulation compared well with the observed frontal movement. Figure 11 shows a vertical cross section through the domain (cross section location shown in Fig. 9) of vertical motion w and equivalent potential temperature θ_e at 0300 UTC. This simulation had no latent heating effects or any way of releasing the convective instability that the frontal convergence is forcing. The squall-line convection is not simulated, and consequently there is no frontal/squall-line separation.

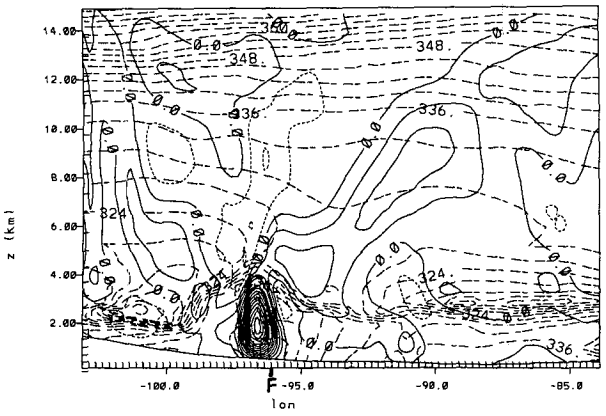

FIG. 11. Vertical cross section from the DRY simulation at 0300 UTC 18 June 1978 of vertical motion w (contour interval is 4 cm s^{-1}, solid lines are contours of positive values and short-dashed lines are contours of negative values) and equivalent potential temperature θ_e (long-dashed lines, contour interval is 3 K). The surface front location is marked by F.

2) MIC SIMULATION

The results of the MIC simulation were very similar to those of the DRY simulation. Overall, the frontal convergence on this scale (20-km grid spacing) was not enough to explicitly force the release of the convective instability. The precipitation associated with the frontal forcing was negligible (not shown). The region of strong frontal forcing moved continuously at approximately 5–10 m s^{-1}. The convergent forcing was not strong enough on that scale to continuously release the instability and was moving too fast to result in any sort of positive feedback.

3) CU SIMULATION

Figure 12 shows the surface analyses of horizontal winds and temperature, MSLP, and the convective precipitation rate from the CU simulation at 0300 UTC 18 June 1978. The frontal and squall-line positions are superimposed on the wind analysis. The frontal position is defined based on the surface wind shift line and temperature analyses, and the leading edge of the squall line is defined as the leading edge of the convective precipitation. At 2100 UTC (not shown), the CU simulation was very similar to the DRY simulation (also not shown), except for a few perturbations associated with the local areas of frontally forced convection over east-central Kansas and western Oklahoma. At 0000 UTC the surface front over Kansas is still disorganized and diffuse in the DRY simulation (not shown), but has concentrated into a narrow line in the CU simulation (not shown), approximately 3 hours earlier than in the DRY simulation. At this time the cumulus parameterization has been activated all along that line, resulting in a continuous "squall line" from eastern Iowa and northern Illinois to the Texas Panhandle. The convection is aligned along the front at this time. By 0300 UTC (Fig. 12) the leading edge of the convective line has moved approximately 300 km southeastward and is now located about 150 km ahead of the surface frontal location. The front is generally moving at 8–12 m s^{-1} at this time and the leading edge of the squall line is moving at ~20 m s^{-1}, although that does not mean that individual "cells" are moving that fast. The trough in the MSLP analysis from the CU simulation has widened and deepened, with the front edge of the trough aligned with the leading edge of the convection and the back edge aligned with the frontal zone. The MSLP analysis and the frontal and convective line locations all compare well with the observed analyses discussed in section 2. The frontal zone and the convective line in the CU simulation have both weakened considerably by 0600 UTC, but the front is

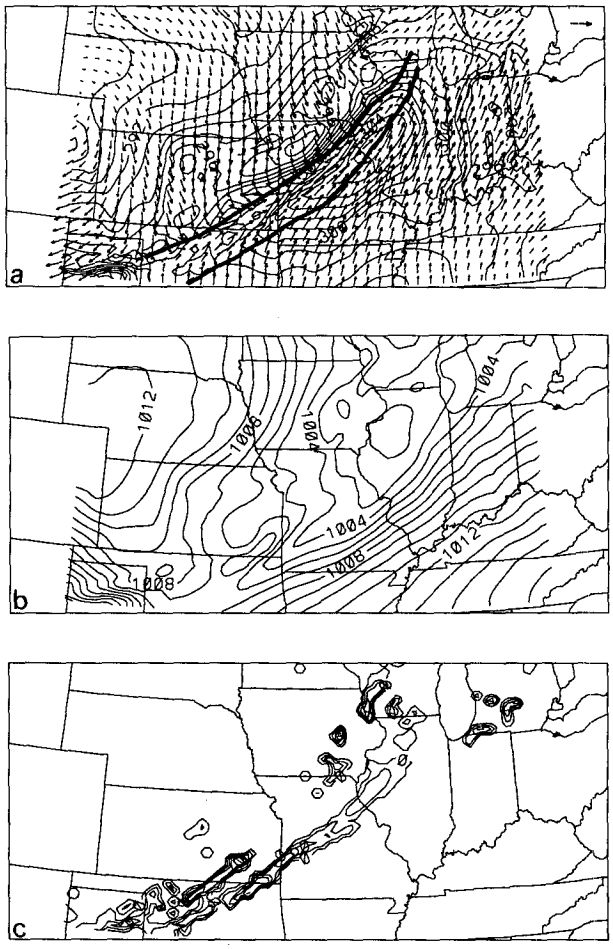

FIG. 12. Surface analyses from CU simulation at 0300 UTC 18 June 1978 of (a) horizontal winds and temperature (contour interval is 1 K); (b) reduced MSLP (contour interval is 1 mb); and (c) convective precipitation rate (contour interval is 0.0003 mm s^{-1}). The lengths of the vectors in (a) are proportional to the speed: the vector in the upper-right corner of (a) is 20 m s^{-1}. The frontal (farther northwest) and squall-line (farther southeast) positions are superimposed on (a).

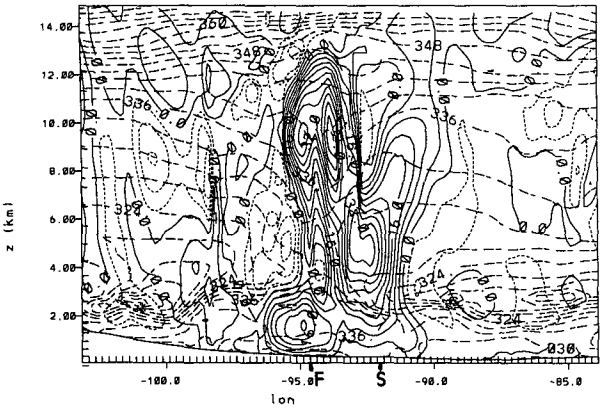

FIG. 13. Vertical cross sections from the CU simulation at 0300 UTC 18 June 1978 of (a) vertical motion w (contour interval is 4 cm s^{-1}, solid lines are contours of positive values and short-dashed lines are contours of negative values) and equivalent potential temperature θ_e (long-dashed lines, contour interval is 3 K). The surface front location is marked by F and the squall-line position (leading edge of convective precipitation) by S.

still oriented along the back edge of the trough and the convective line along the front edge.

The vertical cross section of vertical motion and equivalent potential temperature for the CU simulation at 0300 UTC is shown in Fig. 13 (cross-section location shown in Fig. 9). The vertical motion fields in Fig. 13 are noisy, but they do show the areas of deep vertical motion associated with the cumulus parameterization and their relation to the area of shallow, frontally forced vertical motion. At 2100 UTC the vertical motion forced by the frontal convergence is located in approximately the same place in both the CU (not shown) and DRY (not shown) simulations. By 0300 UTC (Fig. 13) the difference between the frontal and leading-convective-edge positions is clear in the vertical motion field. By 0600 UTC (not shown) the weakening of the convective organization is also apparent. Figure 13 also shows a decrease in the vertical gradient of θ_e caused by the convection, resulting primarily from an erosion of the θ_e minimum at midlevels (3–8 km) and a substantial decrease of θ_e at low levels.

The results from the CU simulation compare well with the observations. The frontal and convective line movements agree well with the observed motions, and the separation of the squall line from the front also appears to be accurately simulated. The mechanism responsible for the separation of the squall line from the front will be analyzed in more detail in Part II.

4) ALL SIMULATION

Figures 14–17 show the surface fields of horizontal winds and temperature, MSLP, and the convective precipitation rate for the ALL simulation at 2100 UTC 17 June and 0000, 0300, and 0600 UTC 18 June 1978. At 2100 UTC the ALL fields (Fig. 14) are very similar to the CU fields (not shown), except in the area over northern Illinois and Wisconsin where the semistationary MCS-like feature has been affected by the explicit microphysical processes in the model. The convection along the squall line, just beginning to show up at 2100 UTC (Fig. 14c), is very similar between the CU and ALL simulations. At 0000 UTC the CU and ALL simulations are still very similar. The squall-line convection shows up clearly in the plot of the convective precipitation rate at 0000 UTC (Fig. 15). There are a few other differences between the CU and ALL simulations at 0300 UTC, although the basic motion of the squall line (defined as the leading edge of the convective precipitation) is the same between the two simulations. The same situation is true at 0600 UTC, with the CU and ALL simulations essentially the same in the vicinity of the squall line. Figure 18 shows the precipitation accumulated from 1800 UTC 17 June to

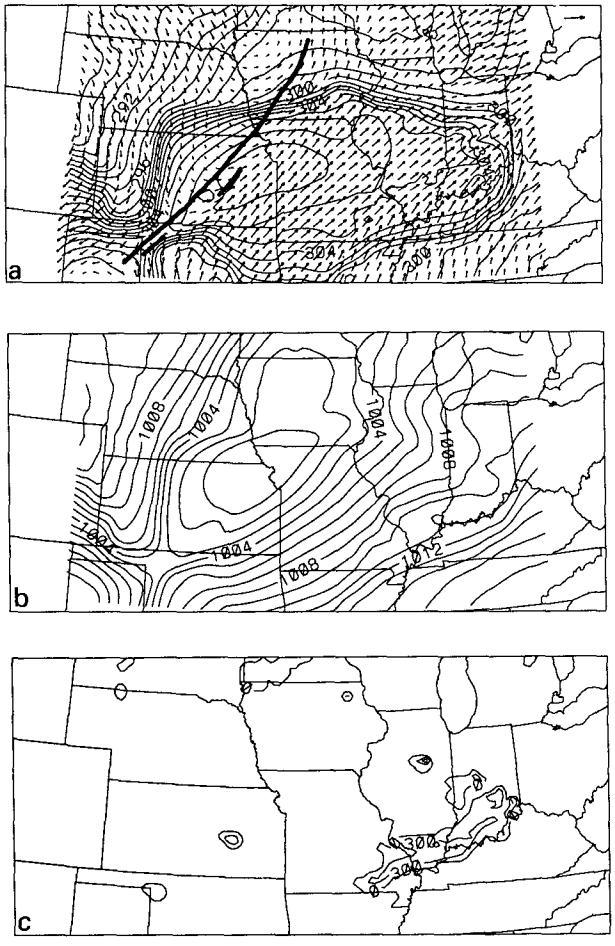

FIG. 14. Analyses from ALL simulation at 2100 UTC 17 June 1978 of (a) surface horizontal winds and temperature (contour interval is 1 K), (b) reduced MSLP (contour interval is 1 mb), and (c) convective precipitation rate (mm s^{-1}, contour interval is 0.0003). The lengths of the vectors in (a) are proportional to the speed: the vector in the upper-right corner of (a) is 20 m s^{-1}. The frontal (farther northwest) and squall-line (farther southeast) positions are superimposed on (a).

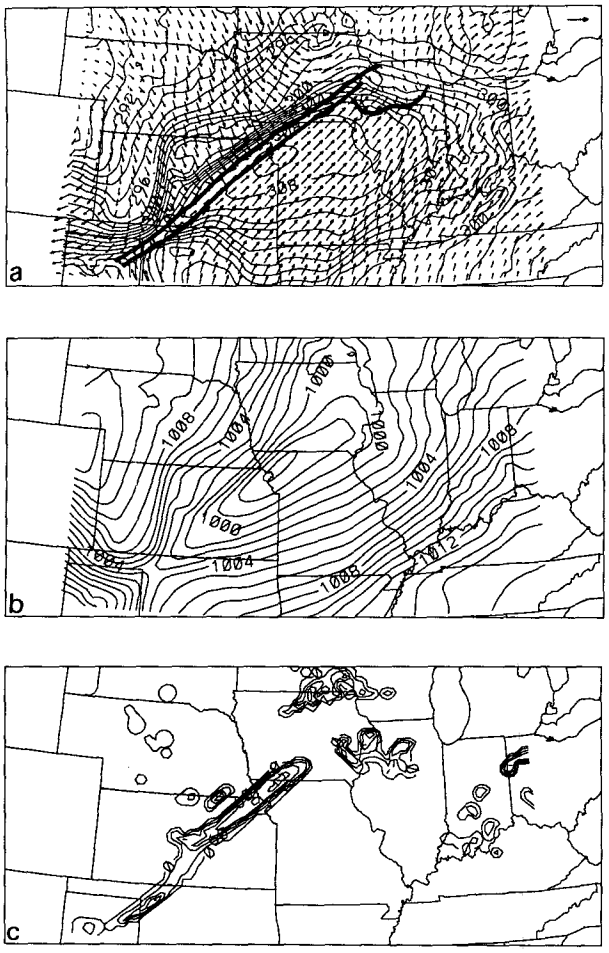

FIG. 15. Same as Fig. 14, except at 0000 UTC 18 June 1978.

0600 UTC 18 June from the convective parameterization scheme. The total amount of convective precipitation from the ALL simulation is very similar to that for the CU simulation (not shown) and approximately half of the observed precipitation for the squall line. Likewise, the area of coverage of the microphysically produced precipitation from the ALL simulation was very similar to that from the MIC simulation (not shown). The microphysically produced precipitation was negligible in the vicinity of the squall line.

The vertical cross sections of vertical motion, equivalent potential temperature, and grid-resolved condensate mixing ratio for the ALL simulation at 2100 UTC 17 June and 0000, 0300, and 0600 UTC 18 June are shown in Figs. 19–22 (cross-section location shown in Fig. 9). The CU and ALL simulations are again very similar at 2100 and 0000 UTC. The cross section of total condensate mixing ratio at 0300 UTC shows the maximum production of condensate at 6–7 km. The outline "looks like" a cross section through a squall line, but in this simulation the leading edge of the squall line is best defined by the leading edge of the convective precipitation, which is slightly ahead of the area of grid-resolved condensate mixing ratio. The lack of significant condensate means that the latent heating effects from the explicit microphysical processes are very small, and thus there is no mechanism to force anvil circulations such as the rear inflow jet.

Overall, the ALL simulation is very similar to the CU simulation. The outline of upper-level total condensate in the ALL simulation is representative of the area of anvil coverage, but the mixing ratios of the condensate in the anvil region are extremely small, mostly less than 0.1 g kg^{-1}. Other studies (Rutledge and Houze 1987) have found stratiform anvil mixing ratios of 0.5–2.0 g kg^{-1}. This result is consistent with the comparison of the DRY and MIC simulations, where the explicit microphysical processes only seemed to become significant where a "spinup" or feedback mechanism existed, as in the MCC development over Wisconsin. The leading edge of the squall line, represented well by the cumulus parameterization scheme, was moving too fast for any feedbacks to develop to reinforce the microphysical processes. As the squall line moved equally fast in nature and apparently did develop an anvil, the problem in the model is perhaps due to a deficiency in the cumulus parameterization

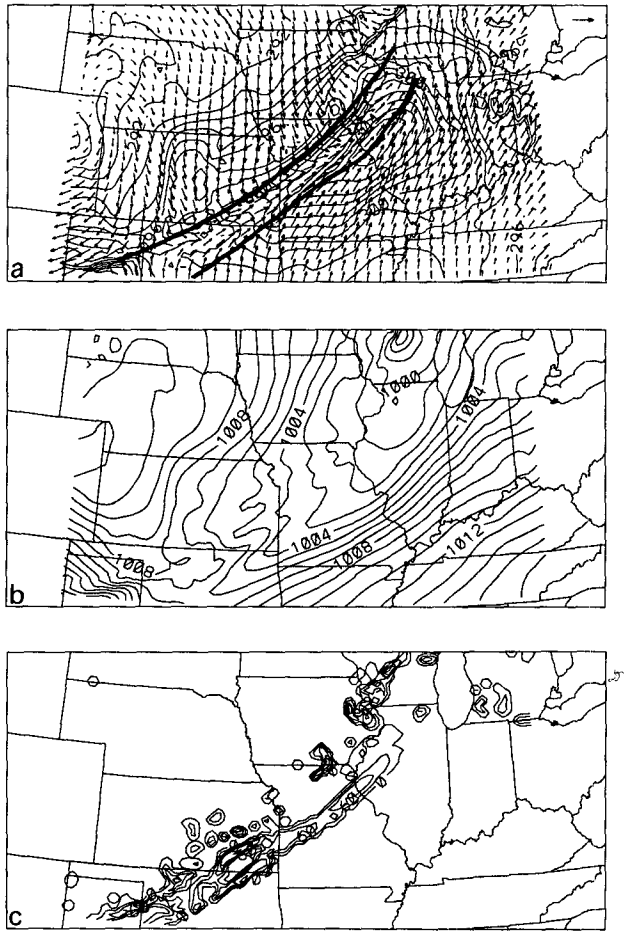

FIG. 16. Same as Fig. 14, except at 0300 UTC 18 June 1978.

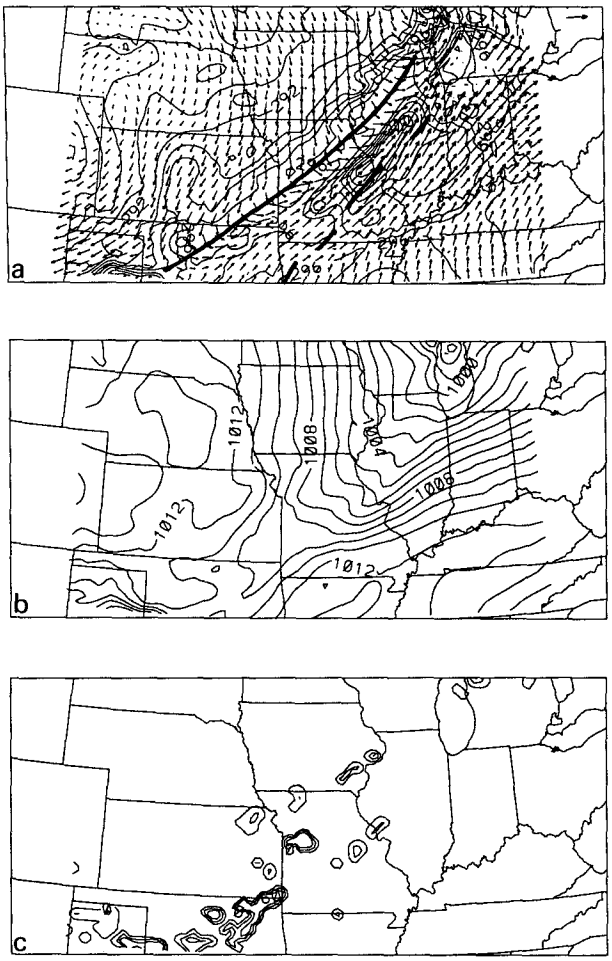

FIG. 17. Same as Fig. 14, except at 0600 UTC 18 June 1978.

scheme. The convective cores in nature act to explicitly produce and transport liquid and frozen condensate upward. The cumulus parameterization scheme as applied in this study does not produce or transport condensate at all, only water vapor mixing ratio. The transported water vapor must then be explicitly converted to condensate by the separate microphysical parameterization in the model. The frontal and squall-line movements in the ALL simulation are summarized and compared to the observations and other simulations in the next section.

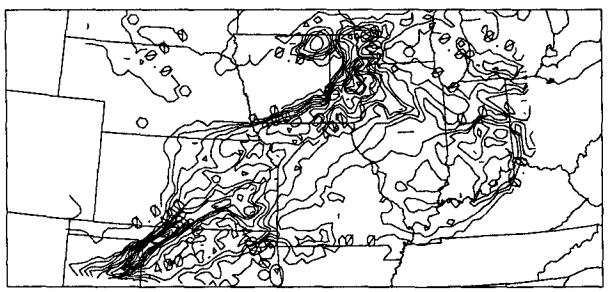

FIG. 18. Precipitation produced by the convective parameterization scheme in the ALL simulation accumulated from 1800 UTC 17 June to 0600 UTC 18 June 1978 (contour interval is 0.1 cm).

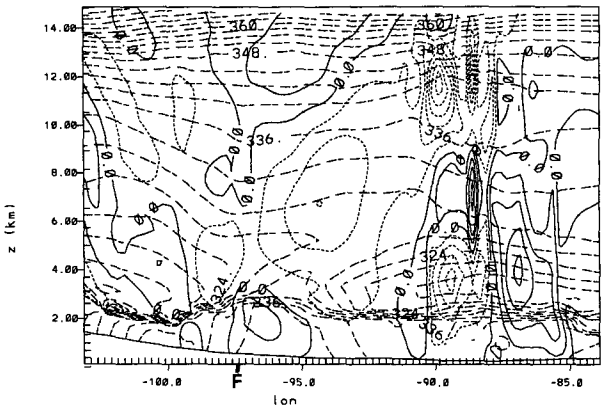

FIG. 19. Vertical cross section from the ALL simulation at 2100 UTC 17 June 1978 of vertical motion w (contour interval is 4 cm s^{-1}, solid lines are contours of positive values and short-dashed lines are contours of negative values) and equivalent potential temperature θ_e (long-dashed lines, contour interval is 3 K). The surface front location is marked by F and the squall-line position (leading edge of convective precipitation) by S.

c. *Summary of numerically simulated frontal and squall-line movements*

The simulations showed that the cumulus parameterization scheme was necessary to simulate the squall-line development and propagation when the 20-km grid increment was used. The model-resolved convergence produced on that scale was not enough to explicitly initiate convection, but the cumulus parameterization scheme did appear to very accurately simulate the squall-line movement. Figure 23 summarizes the relative positions of the front and squall line for

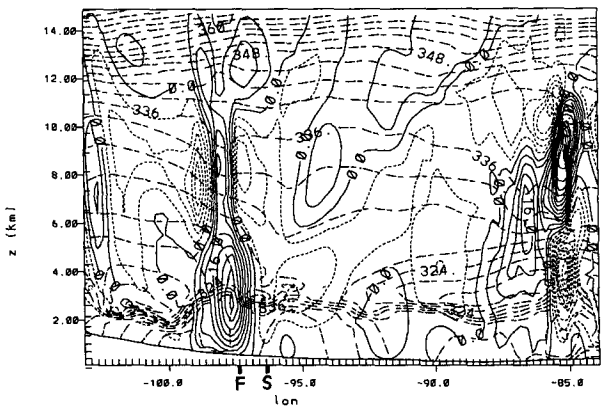

FIG. 20. Same as Fig. 19, except at 0000 UTC 18 June 1978.

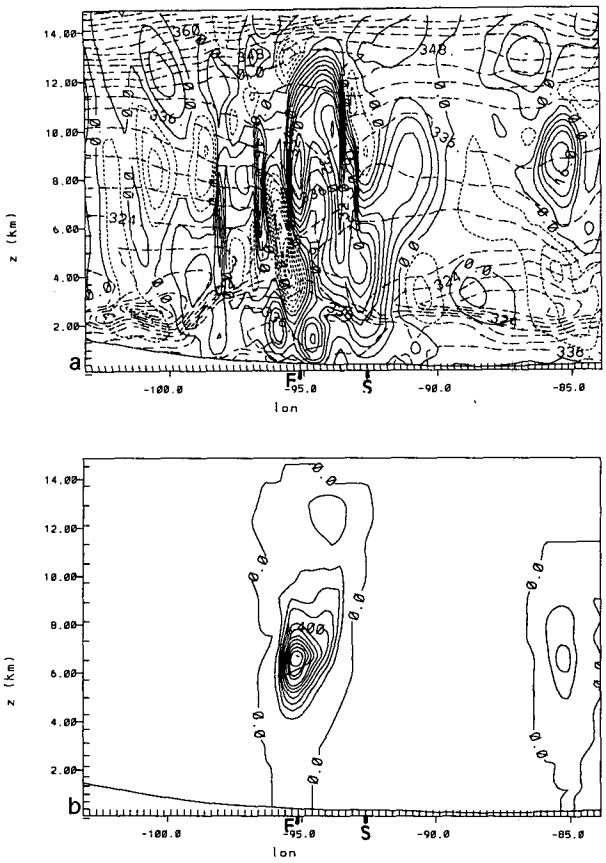

FIG. 21. Vertical cross sections from the ALL simulation at 0300 UTC 18 June 1978 of (a) vertical motion w (contour interval is 4 cm s^{-1}, solid lines are contours of positive values and short-dashed lines are contours of negative values) and equivalent potential temperature θ_e (long-dashed lines, contour interval is 3 K); and (b) condensate mixing ratio (contour interval is 0.1 g kg^{-1}). The surface front location is marked by F and the squall-line position (leading edge of convective precipitation) by S.

the observations and the four basic simulations described previously. Table 2 summarizes the speeds of the front and squall line from the observations and for the same four simulations. The CU and ALL simulations compare very well with the observations. In both simulations, and in the observations, the squall-line convection initially develops along the surface frontal convergence line and then moves out ahead of the front between 0000 and 0600 UTC. By 0600 UTC the frontal/squall-line separation is 300–400 km.

5. Comparison of modeled squall-line structure to other studies

In this section, the structure of the squall line in the ALL simulation will be briefly compared to some of the observed and modeled structures described in section 2. The time series of the MSLP analyses for the ALL simulation (Figs. 14–17) showed an initial pressure fall at the leading edge of the squall line with a relative pressure rise between the passage of the squall line and the front. The increase in pressure in the region between the front and squall line is consistent with observations of the surface mesohigh (Fujita 1955; Zipser 1977; Johnson and Hamilton 1988). The pressure drop just ahead of the area of active convection in the ALL simulation may be construed as the presquall mesolow, but it is due to the subsidence in the propagating internal gravity wave in this case, not the preline, wave-independent, subsidence warming postulated by Hoxit et al. (1976). Zhang and Fritsch (1986, 1988a,b) and Hoxit et al. (1978) also found a similar offset of the convection from the trough axis for the 1977 Johnstown flood case. Zhang and Fritsch (1988b) showed that the trough in that case was due to subsidence at the leading edge of a propagating internal gravity wave. The surface pressure in the ALL simulation is at its lowest just at the edge where the convection is activated in the model, and the presquall mesolow is about 50–100 km wide.

There is no indication in the ALL analyses of a consistent wake-low region. The wake low is generally thought to be due to subsidence warming in the rear-to-front jet below the anvil region (Smull and Houze

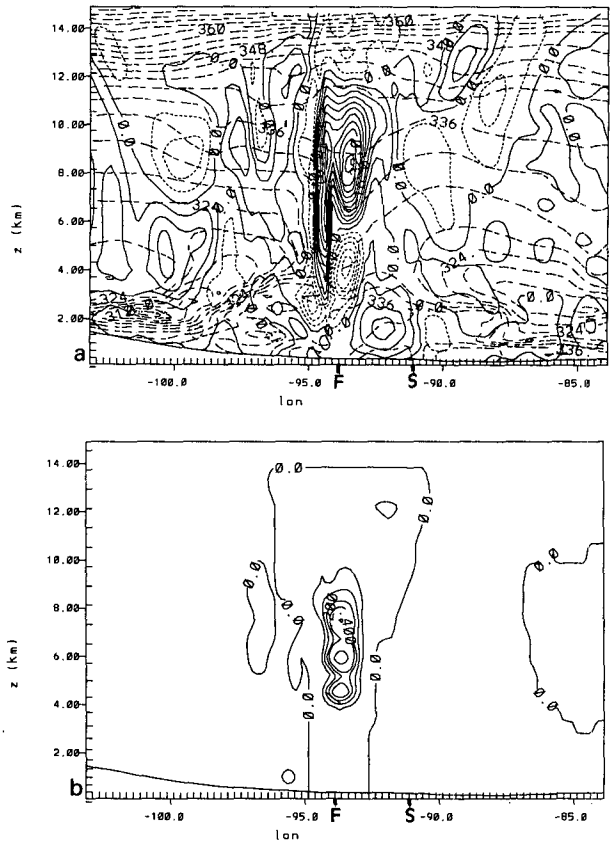

FIG. 22. Same as Fig. 21, except at 0600 UTC 18 June 1978.

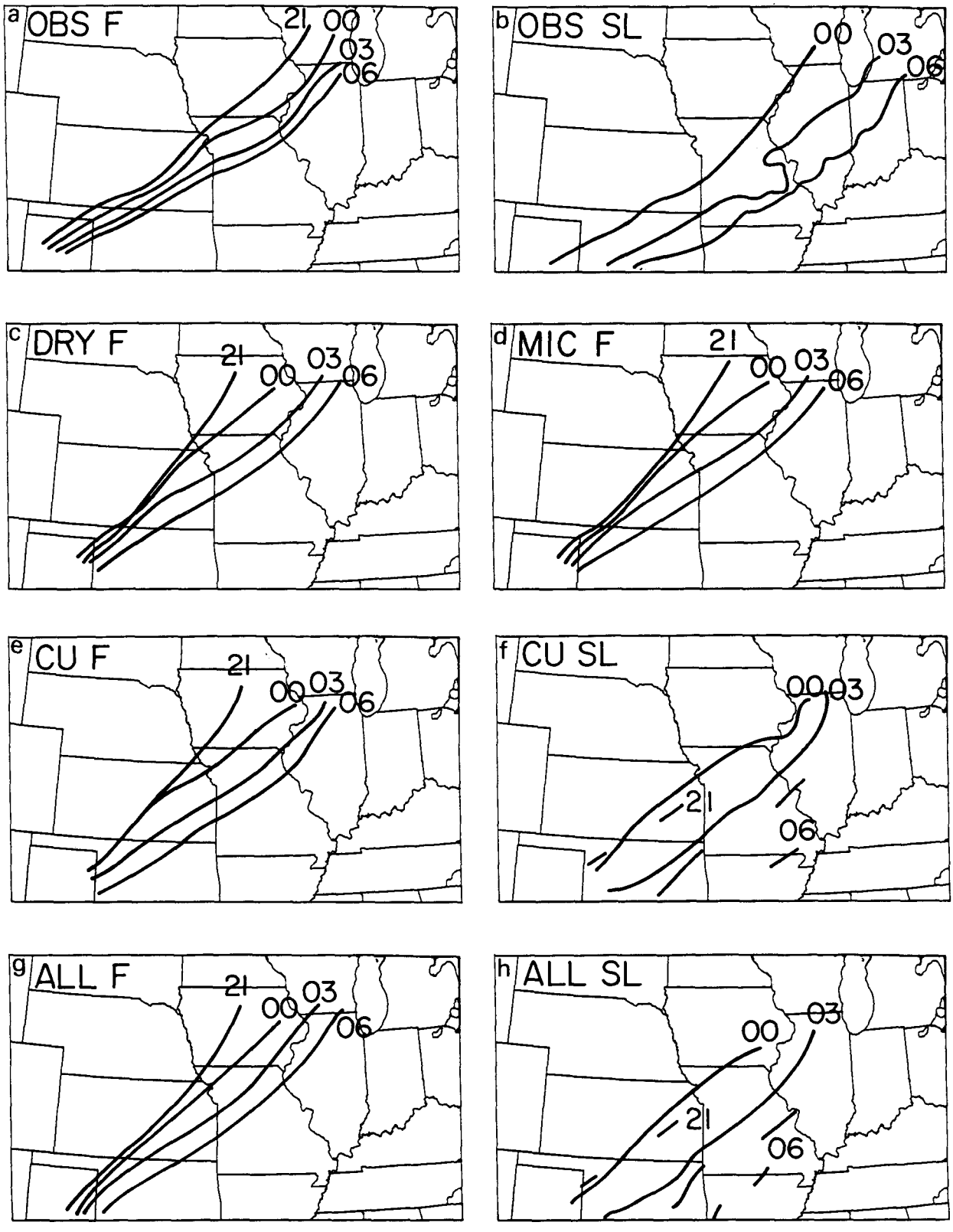

FIG. 23. Three-hour positions of front and squall line for (a) observed front, (b) observed squall line (leading edge of radar echoes), (c) DRY front, (d) MIC front, (e) CU front, (f) CU squall line (leading edge of convective precipitation), (g) ALL front, and (h) ALL squall line (leading edge of convective precipitation).

TABLE 2. Speeds (m s^{-1}) of front and squall line for 3-h periods from the observations and four basic simulations. The speeds in parentheses are the speeds in the region across northern Missouri and are representative of the average speeds of the squall line and front.

	Frontal speeds			Squall-line speeds		
	Time period (UTC hours)					
	21–00	00–03	03–06	21–00	00–03	03–06
Observed	3–11 (8)	3–8 (8)	3–5 (4)		12–21 (12–20)	3–16
DRY	0–11 (5)	1–12 (12)	6–8 (7)			
MIC	0–11 (5)	1–12 (11)	6–8 (8)			
CU	0–11 (7)	5–12 (11)	4–8 (7)	0–5	16–20 (18)	5–24
ALL	3–11 (5)	3–11 (11)	6–8 (7)	0–3	14–20 (18)	5–22

1987; Johnson and Hamilton 1988; Stumpf et al. 1991). The subsidence may be initiated by evaporation from the anvil region (Zipser 1977) or a manifestation of the subsiding rear inflow jet (Johnson and Hamilton 1988). The lack of the wake low in the ALL simulation is probably due to the lack of any significant explicit microphysical effects in the anvil region. The outline of total condensate is representative of the anvil produced only as a result of advective processes. The mixing ratios are almost all less than 0.1 g kg^{-1} and thus indicate that any anvil latent heat production is small. Rutledge and Houze (1987) found anvil condensate mixing ratios of 0.5–2.0 g kg^{-1}. Srivastava et al. (1986) did a Doppler radar study of the anvil region of the squall line on this date, but the anvil region that they studied was semisteady and almost completely detached from the main squall line. They found reflectivities within the anvil region of 20–40 dBZ. According to Rogers (1979), these correspond to precipitation rates of 1–10 mm h^{-1}. Rutledge and Houze (1987) diagnosed anvil regions with reflectivities of 10–30 dBZ as having condensate mixing ratios of 0.4–1.0 g kg^{-1}. Schmidt and Cotton (1990) found that weak environmental shear could result in a weaker rear inflow jet and wake-low region. However, Zhang et al. (1989) found that a strong rear inflow jet and wake low developed in a strong low-level wind shear condition. The vertical wind shear for this case was mostly confined to the layer below 700 mb (Fig. 8).

The ALL simulation does not produce any significant cold air outflow or gust front associated with the squall line. The convective scheme used in these simulations does have a modification for cold downdraft effects (section 3c), which shows up in the profile of convective heating from the convective scheme as cooling below cloud base. As formulated, the intensity of the convective cooling is somewhat arbitrary below cloud base. A deeper or colder layer of cooling might result in a more persistent cold pool or gust front. Although cold air outflow may have occurred along portions of the squall line in reality, it was probably not entirely responsible for the observed squall-line propagation (see section 2). The failure of the model to produce any consistent cold downdrafts is probably due to the 20-km grid interval (and thus its dependence on the cumulus parameterization) and the lack of any significant grid-scale microphysical processes or stratiform anvil production. The production of cold downdrafts on the resolvable scale could then lead to the development of a surface cold pool and gust front.

Zhang and Gao (1989) modeled a squall line using a 25-km grid interval and successfully simulated the formation of a gust front, presquall mesolow, mesohigh, wake low, and rear inflow jet. Zhang and Fritsch (1986, 1988a,b) also successfully modeled many of the meso-β-scale aspects of the 1977 Johnstown flood case. The squall line in Zhang and Gao's case propagated at 14.5 m s^{-1}, slightly slower than the 18 m s^{-1} in this case, but in a similar environment of relatively weak shear aloft. The gravity waves simulated by Zhang and Fritsch (1988b) moved at 25–30 m s^{-1} and were coupled with the convection for a brief period. One difference in those simulations is that they used a version of the Fritsch and Chappell (1980a) cumulus parameterization scheme (hereafter referred to as FC), which has a more detailed calculation of downdraft effects than the scheme used in this study. Features such as the gust front, wake low, and rear inflow jet are all directly caused (in a model) by the successful modeling of resolvable and parameterized downdraft effects and anvil processes such as mesoscale subsidence. However, Tremback (1990) pointed out that the FC cumulus parameterization produces unrealistically large heating rates, with the heating maximum at a very high level. Tremback found that the FC heating rates (from Fritsch and Chappell 1980b) were two to three times those from the observations of a midlatitude squall line (Lewis 1975). Zhang and Fritsch (1986) modified the FC scheme for the Johnstown flood case to have smaller heating rates, but their level of maximum heating was still very high, near 200 mb. Zack et al. (1985) found that the FC scheme initiated convection much more quickly than other schemes and that the large magnitude and high level of parameterized heating in the FC scheme initiated mesoscale ascent and saturation at low-to-middle levels. This then resulted in a much greater interaction between grid scale and parameterized heating effects. The FC scheme appears to initiate

grid-scale convergence and low-to-middle level ascent and saturation because it overestimates the amount and level of the middle-to-upper level convective heating effects.

The failure of the RAMS model to produce a stratiform anvil behind the squall line probably has several causes. First of all, the grid interval in these simulations was 20 km. The 20-km simulations depend on a cumulus scheme to simulate the deep convection, while the explicit microphysics package is included to simulate any grid-scale microphysics conversion processes. We doubt that there is as much interaction between the cumulus parameterization scheme and the microphysical processes as there should be. The cumulus scheme is parameterizing the overall effects of convection on the temperature and mixing ratio fields. The moisture fluxes produced by the convective parameterization may not be as strong as they need to be to maintain the grid-scale anvil microphysical processes, and they may not be consistent with the ice phase processes that occur in the explicit microphysics package. The cumulus parameterization scheme only transports water-vapor mixing ratio upward, not liquid or frozen condensate. Any condensate must then be produced in situ by the parameterized microphysical processes. There will thus be a time lag (perhaps too long for this fast-moving line) in the appearance of any liquid or ice phase constituents that result from the convective moisture transports.

The cross sections of equivalent potential temperature, θ_e, shown in Figs. 19–22 are consistent with the analyses of other investigators. There is a minimum of θ_e ahead of the squall line at a height of about 3–4 km. The strong minimum is consistent with the results found by Barnes and Seickman (1984) for fast-moving lines. The vertical θ_e gradient behind the squall line is also decreased, with lower values of θ_e at the surface and an increase in the midlevel θ_e, consistent with the results of Ogura and Liou (1980).

Potential vorticity (PV) is another variable that is modified by the passage of a squall line. Hertenstein and Schubert (1990) analyzed data from the PRE-STORM experiment and also used a simple semigeostrophic analytic model to show that a squall line leaves in its wake a positive PV anomaly at low-to-middle levels and a negative anomaly aloft. The positive anomaly is located below the level of the maximum heating. Figure 24 shows the PV analyses for the ALL simulation at 0600 UTC in the same vertical cross section as in the previous figures (shown in Fig. 10). The potential vorticity was defined as

$$\mathrm{PV} = \left(f + \frac{\partial v}{\partial x} - \frac{\partial u}{\partial y}\right)\frac{\partial \theta}{\partial z}\frac{1}{\rho g} - \frac{\partial v}{\partial z}\frac{\partial \theta}{\partial x}\frac{1}{\rho g} + \frac{\partial u}{\partial z}\frac{\partial \theta}{\partial y}\frac{1}{\rho g}, \quad (5.2)$$

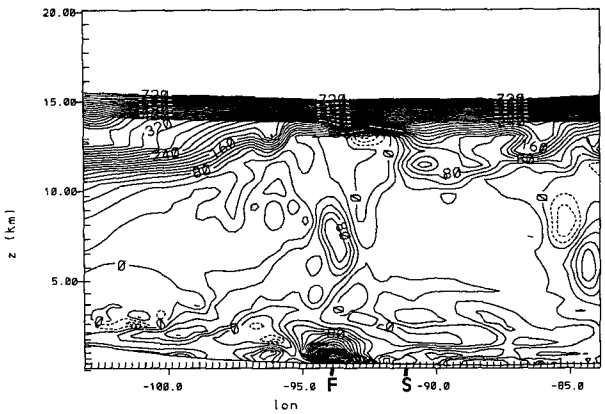

FIG. 24. East–west cross section at 0600 UTC of potential vorticity (K s m g^{-1}, contour interval is 2×10^{-8}, dashed lines are negative value contours) in the ALL simulation.

where f is the Coriolis parameter, u and v are the horizontal velocities in the x and y directions, ρ is the density, and g is the gravitational acceleration. A general increase in PV below about 5 km and a decrease above that is apparent behind the squall line, as well as a local maximum at a height of about 7–8 km. This maximum is located behind the leading convective region. The PV maximum must be mostly a result of the heating produced by the cumulus parameterization scheme as it is also evident in the CU simulation (not shown). The level of maximum heating at 0600 UTC was deduced to be slightly higher than 10 km, and the positive PV anomaly is located just below it, as predicted by theory.

6. Summary

The squall line in this study occurred on 17–18 June 1978. Srivastava et al. (1986) did a Doppler radar study of part of the anvil region at the northern end of the squall line. This squall line developed very explosively between 2100 UTC 17 June and 0000 UTC 18 June 1978, with a continuous line of convection extending from Illinois to the Texas Panhandle by 0000 UTC. The squall line was initially triggered by the strong convergence across a surface cold front, but then moved away from the cold front between 0000 and 0600 UTC. The separation between the front and the squall line was about 200 km by 0300 UTC and 300–400 km by 0600 UTC. Both Srivastava et al. and Thomas Matejka (personal communication, discussed in section 2) noted that the squall line propagated discretely, with new convection forming 25–100 km ahead of the gust front, although their observations cannot be verified independently.

The RAMS model developed at Colorado State University was used for the modeling simulations described in this study and was described in section 3c.

A nonhydrostatic version of the model was used, with a coarse grid spacing of 80 km and a fine grid spacing of 20 km. The model simulations were all initialized at 1200 UTC 17 June 1978 from an analysis of the NMC spectral model data and available rawinsonde and surface observations. Four different simulations were completed in an attempt to isolate the effects of the cumulus parameterization scheme (a modified Kuo-type scheme) and the grid-scale microphysical processes.

The simulation of the squall line in the ALL and CU simulations (with 20-km grid intervals) compared well with the observed squall-line movements. Both simulations used a modified Kuo-type cumulus parameterization scheme, and the ALL simulation also included the grid-scale microphysical processes. The CU simulation included grid-scale latent heating effects and production of cloud water, but no other parameterization of grid-scale precipitation processes. The squall line in the ALL and CU simulations initially developed in the zone of strong surface frontal convergence between 2100 and 0000 UTC. By 0000 UTC the squall line was evident in the model as a solid line of convection extending from Iowa to the Texas Panhandle. Between 0000 and 0600 UTC the squall line separated from the front in the ALL and CU simulations, moving approximately 200 km ahead of the front by 0300 UTC and 300–400 km ahead of the front by 0600 UTC. The positions of the simulated squall line and front in the CU and ALL simulations compared well with the observed positions of the squall line and front, as summarized in Fig. 23. The squall-line convection did not form in the MIC simulation at all, where only the grid-scale microphysical processes were represented. A cumulus parameterization scheme was necessary to simulate the effects of deep cumulus convection with the 20-km grid spacing.

Some aspects of the meso-α- and meso-β-scale structure of the squall line in the CU and ALL simulations compared very well to observed squall line structures, while other aspects did not. The presquall mesolow and convective mesohigh regions were consistent in the model analyses, although weaker than most cases reported in the literature. There was no indication of a wake-low region, rear inflow jet, or gust front processes in these modeling simulations. The lack of a wake-low region and rear inflow jet is due to the failure of the model to produce any significant heating or microphysical processes in the anvil region, and also possibly due to the weak shear. It is not clear whether this is due to a deficiency in the model microphysical processes or the cumulus parameterization scheme, or to an otherwise improper simulation that then inhibited the anvil formation. The squall line moved at approximately 18 m s^{-1} in the model simulations and was moving too fast for any anvil-related heating processes to consolidate in the model. The grid-scale microphysical processes in the model simulations were only significant in regions of strong upward motion (along the convective core region of the squall line) or in semistationary regions where the heating and precipitation processes had a positive feedback effect (similar to conventional CISK). The cumulus parameterization scheme may be deficient in that it does not produce or transport liquid or frozen condensate, only water-vapor mixing ratio, and there is thus not as much interaction between the cumulus parameterization scheme and the microphysical processes as there should be. The lack of the production of a gust front or consistent cold downdraft processes is also tied to the apparent lack of significant grid-scale microphysical processes. The cumulus parameterization scheme used in these simulations does have a modification for cold downdraft effects, but their effects were small in these simulations.

Zhang and Fritsch (1986, 1988a,b), Zhang et al. (1989), and Zhang and Gao (1989) were able to simulate the rear inflow, wake-low region, and cold downdrafts and gust front in a squall-line simulation with a fine grid interval of 25 km. They used a modified version of the Fritsch and Chappell (1980a,b) (FC) cumulus parameterization on their fine grid that has a more explicit calculation of downdraft effects. As previously discussed, the original FC scheme produces excessive amounts of heating at unreasonably high levels (compared with observations). The excessive heating can apparently induce low-to-middle level ascent and saturation. The FC scheme may thus be effectively parameterizing aspects of both the convective and stratiform heating, although in the above cases it was also used in addition to the grid-scale condensational processes.

The issue of the predictability of meso-α- and meso-β-scale features in models from standard synoptic information has been posed by Anthes et al. (1982). As mentioned above, Zhang and Fritsch (1986, 1988a,b), Zhang et al. (1989), and Zhang and Gao (1989) were able to simulate many of the meso-β-scale features associated with a squall line in a model with a fine grid interval of 25 km. Several of the meso-β-scale features of the squall line were also simulated in the model results described in this study, such as the presquall mesolow and mesohigh. These results, and those mentioned above, are promising in that they imply that smaller-scale features and structures associated with convection can indeed be modeled even when only meso-α- and synoptic-scale information is available for model initialization. However, Zhang and Fritsch pointed out that the predictability of these features will be better in situations where the system is more strongly forced by the environmental dynamics than the thermodynamics. Such was the case for the 17 June 1978 squall line.

In Part II (Cram et al. 1991), the mechanism for the propagation of the squall line is discussed. The

modeling study suggests that the squall line propagated as a deep tropospheric internal gravity wave in a wave–CISK-like process. An additional simulation with a 5-km grid spacing and without the inclusion of the cumulus parameterization scheme is also discussed in the appendix to Part II.

Acknowledgments. This work was completed while the first author was a graduate student in the Department of Atmospheric Science at Colorado State University and was supported by a NASA Training Grant Fellowship (NASA Grant NGT-06-002-802). Partial support was also provided by the Army Research Office (ARO) Center for Geosciences, Contract DAAL03-86-K-0175. The numerical simulations described in this paper were mostly completed on the CRAY X-MP computer at the National Center for Atmospheric Research (under National Science Foundation Grant ATM-8814913). The National Center for Atmospheric Research is sponsored by the National Science Foundation. Data obtained from the NCAR data archives were used to initialize the model simulations and for verification analyses. Most of the preliminary work for this study, including extensive model debugging, was completed on the CYBER 205 computer at Colorado State University. Craig Tremback, Bob Walko, Mike Moran, Jerry Schmidt, and Rolf Hertenstein are thanked for many helpful discussions and suggestions over the course of this work. Thomas Matejka is thanked for providing his personal observations of the 17–18 June 1978 squall line. John Brown is thanked for providing more complete sounding data. Dallas McDonald is thanked for typing the manuscript. Judy Sorbie-Dunn drafted several of the figures.

REFERENCES

Anthes, R. A., Y.-H. Kuo, S. G. Benjamin, and Y.-F. Li, 1982: The evolution of the mesoscale environment of severe local storms: Preliminary modeling results. *Mon. Wea. Rev.*, **110**, 1187–1213.

Barnes, G. M., and K. Seickman, 1984: The environment of fast- and slow-moving tropical mesoscale convective cloud line. *Mon. Wea. Rev.*, **112**, 1782–1294.

Barnes, S. L., 1964: A technique for maximizing details in numerical weather map analysis. *J. Appl. Meteor.*, **3**, 396–409.

——, 1973: Mesoscale objective map analysis using weighted time-series observations. NOAA Tech. Memo. ERL NSSL-62, National Severe Storms Laboratory, Norman, OK, 38 pp.

Bluestein, H. B., and M. H. Jain, 1985: Formation of mesoscale lines of precipitation: Severe squall lines in Oklahoma during the spring. *J. Atmos. Sci.*, **42**, 1711–1732.

Chang, C. B., D. J. Perkey, and C. W. Kreitzberg, 1981: A numerical case study of the squall line of 6 May 1975. *J. Atmos. Sci.*, **38**, 1601–1615.

Cotton, W. R., C. J. Tremback, and R. L. Walko, 1988: CSU RAMS—a cloud model goes regional. *Proc. NCAR Workshop on Limited-Area Modeling Intercomparison*, Boulder, NCAR, 202–211.

Cram, J. M., 1990: Numerical simulation and analysis of the propagation of a prefrontal squall line. Ph.D. dissertation. Colorado State University, Ft. Collins, 330 pp.

——, R. A. Pielke, and W. R. Cotton, 1992: Numerical simulation and analysis of a prefrontal squall line. Part II: Propagation of the squall line as an internal gravity wave. *J. Atmos. Sci.*, **49**, 209–225.

Fritsch, J. M., and C. F. Chappell, 1980a: Numerical prediction of convectively driven mesoscale pressure systems. Part I: Convective parameterization. *J. Atmos. Sci.*, **37**, 1722–1733.

——, and ——, 1980b: Numerical prediction of convectively driven mesoscale pressure systems. Part II: Mesoscale model. *J. Atmos. Sci.*, **37**, 1734–1762.

Fujita, T. T., 1955: Results of detailed synoptic studies of squall lines. *Tellus VII*, **4**, 405–436.

——, 1981: Tornadoes and downbursts in the context of generalized planetary scales. *J. Atmos. Sci.*, **38**, 1511–1534.

Hane, C. E., 1973: The squall line thunderstorm: Numerical experimentation. *J. Atmos. Sci.*, **30**, 1672–1690.

——, C. J. Kessinger, and P. S. Ray, 1987: The Oklahoma squall line of 19 May 1977. Part II: Mechanisms for maintenance of the region of strong convection. *J. Atmos. Sci.*, **44**, 2866–2883.

Hertenstein, R. F. A., and W. H. Schubert, 1991: Potential vorticity anomalies associated with squall lines. *Mon. Wea. Rev.*, **119**, 1663–1672.

Hoxit, L. R., C. F. Chappell, and J. M. Fritsch, 1976: Formation of mesolows and pressure troughs in advance of cumulonimbus clouds. *Mon. Wea. Rev.*, **104**, 1419–1428.

——, R. A. Maddox, C. F. Chappell, F. L. Zuckerberg, H. M. Mogul, J. Jones, D. R. Greene, R. E. Saffle, and R. A. Scofield, 1978: Meteorological analysis of the Johnstown, Pennsylvania, flash flood, 19–20 July 1977. NOAA Tech. Rep. ERL 401-APCL43, 71 pp.

Johnson, R. H., and P. J. Hamilton, 1988: The relation of surface pressure features to the precipitation and air flow structure of an intense midlatitude squall line. *Mon. Wea. Rev.*, **116**, 1444–1472.

Kuo, H. L., 1965: On the formation and intensification of tropical cyclones through latent heat release by cumulus convection. *J. Atmos. Sci.*, **22**, 40–63.

——, 1974: Further studies of the parameterization of the influence of cumulus convection on the large-scale flow. *J. Atmos. Sci.*, **31**, 1232–1240.

Lafore, J. P., and M. W. Moncrieff, 1989: A numerical investigation of the organization and interaction of the convective and stratiform regions of a tropical squall line. *J. Atmos. Sci.*, **46**, 521–544.

Lewis, J. M., 1975: Test of the Ogura-Cho model on a pre-frontal squall line case. *Mon. Wea. Rev.*, **103**, 764–778.

Maddox, R. A., 1980: Mesoscale convective complexes. *Bull. Amer. Meteor. Soc.*, **61**, 1374–1387.

Molinari, J., 1985: A general form of Kuo's cumulus parameterization. *Mon. Wea. Rev.*, **113**, 1411–1416.

Moncrieff, M. W., and M. J. Miller, 1976: The dynamics and simulation of tropical cumulonimbus and squall lines. *Quart. J. Roy. Meteor. Soc.*, **102**, 373–394.

Nicholls, M. E., 1987: A comparison of the results of a two-dimensional numerical simulation of a tropical squall line with observations. *Mon. Wea. Rev.*, **115**, 3055–3077.

——, and M. J. Weissbluth, 1988: A comparison of two-dimensional and quasi three-dimensional simulations of a tropical squall line. *Mon. Wea. Rev.*, **116**, 2437–2452.

——, R. H. Johnson, and W. R. Cotton, 1988: The sensitivity of two-dimensional simulations of tropical squall lines to environmental profiles. *J. Atmos. Sci.*, **45**, 3625–3649.

Ogura, Y., and M.-T. Liou, 1980: The structure of a mid-latitude squall line: A case study. *J. Atmos. Sci.*, **37**, 553–567.

Orlanski, J., and B. B. Ross, 1984: The evolution of an observed cold front. Part II: Mesoscale dynamics. *J. Atmos. Sci.*, **41**, 1669–1703.

——, and ——, 1986: Low-level updrafts in stable layers forced by convection. *J. Atmos. Sci.*, **43**, 997–1005.

Rogers, R. R., 1979: *A Short Course in Cloud Physics.* 2d ed. Pergamon, 235 pp.

Rotunno, R., J. B. Klemp, and M. L. Weisman, 1988: A theory for strong, long-level squall lines. *J. Atmos. Sci.,* **45,** 463–485.

Rutledge, S. A., and R. A. Houze, Jr., 1987: A diagnostic modeling study of the trailing stratiform region of a midlatitude squall line. *J. Atmos. Sci.,* **44,** 2640–2656.

Schmidt, J. M., and W. R. Cotton, 1990: Interactions between upper and lower tropospheric gravity waves on squall line structure and maintenance. *J. Atmos. Sci.,* **47,** 1205–1222.

Smull, B. F., and R. A. Houze, Jr., 1987: Rear inflow in squall lines with stratiform precipitation. *Mon. Wea. Rev.,* **115,** 2869–2889.

Srivastava, R. C., T. J. Matejka, and T. J. Lorello, 1986: Doppler radar study of the trailing anvil region associated with a squall line. *J. Atmos. Sci.,* **43,** 356–377.

Stumpf, G. J., R. H. Johnson, and B. F. Smull, 1991: The wake low in a midlatitude mesoscale convective system having complex organization. *Mon. Wea. Rev.,* **119,** 134–158.

Thorpe, A. J., M. J. Miller, and M. W. Moncrieff, 1982: Two-dimensional convection in non-constant shear: A model of midlatitude squall lines. *Quart. J. Roy. Meteor. Soc.,* **108,** 739–762.

Tremback, C. J., 1990: Numerical simulation of a mesoscale convective complex: Model development and numerical results. Ph.D. dissertation. Colorado State University, Ft. Collins, 247 pp.

——, G. J. Tripoli, R. Arritt, W. R. Cotton, and R. A. Pielke, 1986: The Regional Atmospheric Modelling System. *Proc. Int. Conf. on Development and Application of Computer Techniques to Environmental Studies,* Los Angeles, P. Zannetti, Ed., Computational Mechanics Publications, 601–607.

Tripoli, G. J., and W. R. Cotton, 1989a: Numerical study of an observed orogenic mesoscale convective system. Part 1: Simulated genesis and comparison with observations. *Mon. Wea. Rev.,* **117,** 273–304.

——, and ——, 1989b: Numerical study of an observed orogenic mesoscale convective system. Part 2: Analysis of governing dynamics. *Mon. Wea. Rev.,* **117,** 305–328.

Zack, J. W., M. L. Kaplan, and V. C. Wong, 1985: A comparison of the prognostic performance of several cumulus parameterizations in mesoscale simulations of the 10 April 1979 Sesame I case. Preprints, *Seventh Conf. on Numerical Weather Prediction,* Montreal, Amer. Meteor. Soc., 415–422.

Zhang, D.-L., and J. M. Fritsch, 1986: Numerical simulation of the meso-β-scale structure and evolution of the 1977 Johnstown flood. Part I: Model description and verification. *J. Atmos. Sci.,* **43,** 1913–1943.

——, and ——, 1987: Numerical simulation of the meso-β-scale structure and evolution of the 1977 Johnstown flood. Part II: Inertially stable warm-core vortex and the mesoscale convective complex. *J. Atmos. Sci.,* **44,** 2593–2612.

——, and ——, 1988a: Numerical sensitivity experiments of varying model physics on the structure, evolution, and dynamics of two mesoscale convective systems. *J. Atmos. Sci.,* **45,** 261–293.

——, and ——, 1988b: Numerical simulation of the meso-β-scale structure and evolution of the 1977 Johnstown Flood. Part III: Internal gravity waves and the squall line. *J. Atmos. Sci.,* **45,** 1252–1268.

——, and K. Gao, 1989: Numerical simulations of an intense squall line during 10–11 June 1985 PRE-STORM. Part II: Rear inflow, surface pressure perturbations, and stratiform precipitation. *Mon. Wea. Rev.,* **117,** 2067–2094.

——, E.-Y. Hsie, and M. W. Moncrieff, 1988: A comparison of explicit and implicit predictions of convective and stratiform precipitating weather systems with a meso-β-scale numerical model. *Quart. J. Roy. Meteor. Soc.,* **114,** 31–60.

——, K. Gao, and D. B. Parsons, 1989: Numerical simulations of an intense squall line during 10–11 June 1985 PRE-STORM. Part I: Model verification. *Mon. Wea. Rev.,* **117,** 960–994.

Zipser, E. J., 1977: Mesoscale and convective-scale downbursts as distinct components of squall-line structure. *Mon. Wea. Rev.,* **105,** 1568–1589.